Asian Journal of Pharmaceutical Sciences 15 (2020) 374–384

Available online at www.sciencedirect.com

ScienceDirect

journal homepage: www.elsevier.com/locate/AJPS

Original Research Paper

Critical physicochemical attributes of chitosan nanoparticles admixed lactose-PEG 3000 microparticles in pulmonary inhalation

Nasser Alhajj[a,b], *Zabliza Zakaria*[a,b], *Idanawati Naharudin*[a,b], *Fakhrul Ahsan*[c], *Wenji Li*[d], *Tin Wui Wong*[a,b,*]

[a] *Non-Destructive Biomedical and Pharmaceutical Research Centre, iPROMISE, Universiti Teknologi MARA, Puncak Alam 42300, Malaysia*
[b] *Particle Design Research Group, Faculty of Pharmacy, Universiti Teknologi MARA, Puncak Alam 42300, Malaysia*
[c] *Department of Pharmaceutical Sciences, School of Pharmacy, Texas Tech University Health Sciences Center, Amarillo 79106, USA*
[d] *Department of Integrated Traditional Chinese and Western Medicine, Medical College, Yangzhou University, Yangzhou 225001, China*

ARTICLE INFO

Article history:
Received 3 December 2018
Revised 21 January 2019
Accepted 1 February 2019
Available online 19 March 2019

Keywords:
Chitosan
Inhalation
Nanoparticle
Pulmonary

ABSTRACT

Chitosan nanoparticles are exhalation prone and agglomerative to pulmonary inhalation. Blending nanoparticles with lactose microparticles (~5 μm) could mutually reduce their agglomeration through surface adsorption phenomenon. The chitosan nanoparticles of varying size, size distribution, zeta potential, crystallinity, shape and surface roughness were prepared by spray drying technique as a function of chitosan, surfactant and processing conditions. Lactose-polyethylene glycol 3000 (PEG3000) microparticles were similarly prepared. The chitosan nanoparticles, physically blended with fine lactose-PEG3000 microparticles, exhibited a comparable inhalation performance with the commercial dry powder inhaler products (fine particle fraction between 20% and 30%). Cascade impactor analysis indicated that the aerosolization and inhalation performance of chitosan nanoparticles was promoted by their higher zeta potential and circularity, and larger size attributes of which led to reduced inter-nanoparticulate aggregation and favored nanoparticles interacting with lactose-PEG3000 micropaticles that aided their delivery into deep and peripheral lungs.

* Corresponding author. Non-Destructive Biomedical and Pharmaceutical Research Centre, iPROMISE, Universiti Teknologi MARA, Puncak Alam 42300, Malaysia. Tel.: +60 3 32584691.
E-mail address: wongtinwui@salam.uitm.edu.my (T.W. Wong).
Peer review under responsibility of Shenyang Pharmaceutical University.

https://doi.org/10.1016/j.ajps.2019.02.001

1. Introduction

The lung offers an ideal way for local and systemic drug delivery because of its large surface area, high permeability attribute, and reduced first pass metabolism level [1]. Further, drug administration via the lung is a non-invasive approach and possible for self-administration.

Nanoparticulate delivery system has received a widespread interest for use to deliver therapeutics for different diseases such as cancer and infection [2,3]. Nanoparticles enable therapeutic agents to be delivered in a targeted fashion. They also improve drug solubility, extend drug half-life, improve therapeutic index, and reduce drug immunogenicity [4,5]. The nanoparticles (~600 nm) can penetrate the mucus barrier of biological interface thereby raising the drug bioavailability [6,7].

Delivering nanoparticles via the lung gains much interests for several reasons. First, nano-size particles can cross the cellular barrier independent of the energy supply. Second, these nanoparticles can be designed to be taken up by macrophages for delivery of drugs directly to bacteria and thus treat diseases such as tuberculosis. The nanoparticles can be used to deliver macromolecular drugs such as peptide and protein through the lung for the treatment of systemic or local diseases [8]. They are deemed to be effective for lung cancer treatment in association with improved drug accumulation inside the tumors due to nanoparticulation of the therapeutics facilitating their passive as well as active delivery [5]. Nanoparticles are also used to treat mucus hypersecretion and severe inflammatory lung diseases namely asthma, cystic fibrosis and chronic obstructive pulmonary disease. This is ascribed to their ability to provide sustained drug release, overcome airway hyper-secretion and target diseased cells or tissues through matrix decoration with homing device [9].

However, nanoparticles have the disadvantages of being exhaled from lungs after pulmonary administration. The inhaled particles should have an aerodynamic diameter (D_{ae}) between 1 and 5 μm in order to enable the drugs being deposited in the deep lungs. The particles with $D_{ae} > 5$ μm will be impacted on the large airway whereas particles with $D_{ae} < 0.5$ μm will be exhaled [10]. Several approaches have been developed to form nanoparticles with suitable aerodynamic diameters for lung delivery. The first approach involves the process of nanoagglomeration where the nanoparticles are agglomerated into larger and relatively porous Trojan particles or nanocomposites to improve the aerodynamic characteristics for lung deposition. The Trojan particles are hollow microparticles in which the shell is made of layers of nanoparticles agglomerations [11,12]. Unlike Trojan particles, the internal core of nanocomposites is occupied with nanoparticles in a loose packing geometry [13,14]. The ability of nanoagglomerate systems to have the nanoparticles released and redispersed *in vivo* remains uncertain [15,16]. To resolve this problem, a second approach is developed.

In the second approach, the nanoparticles are spray-dried with carbohydrate to form inhalable nanoparticles loaded microparticles. Following particle deposition onto the targeted surface of pulmonary epithelium, the carbohydrate will dissolve and facilitate the dispersion of nanoparticles [17–22]. Nonetheless, such dosage forms run the risks of inadequate nanoparticle release as a function of microcarrier/nanoparticle material property and processing condition [23,24]. Further, nanoparticle size can change during the microencapsulation process [22], suggesting the size-dependent biological performances of nanoparticles can be affected by nano-to-micro scale transformation. With reference to thermolabile substances, spray-freeze-drying is used as the substitute technique to improve the stability of both the polymer and the drug [25]. However, the process of freezing is accompanied by risks of phase separation into ice and cryoconcentrate. The cryoconcentrate phase contains nanoparticles and they are prone to agglomeration making the redispersion of nanoparticles difficult [26,27].

The current approaches of producing inhalable nanoparticles have several drawbacks. Firstly, they require meticulous efforts in the formulation steps. This problem is intensified by the fact that each formulation is only likely to be applicable to a specific nanoparticle type. Further, the microscale particles are known to face issues of poor flowability and dispersibility in association with their cohesive nature. The coarse carriers are required as a part of externally added formulation. The attachment force between small microscale and coarse carrier particles is difficult to be modulated for deep lung deposition of drugs since it depends on a myriad of parameters belonging to both particles [28]. This increases the risk of losing drugs in the upper airway.

In this study, we aim to develop a new delivery approach of nanoparticles via the pulmonary route possibly for use in lung cancer treatment. A physical mixture of solid nanoparticles with small microscale carrier particles is produced as the model of dosage form. The nanoparticles will spread on the surfaces of the microparticles. This nano-on-microparticle distribution is hypothesized to have dual effects. First, it will prevent nanoparticles from agglomeration. Second, the nanoparticles will work as a spacer between the microparticles and prevent microparticles from agglomeration as well. Achieving our goal will provide a dissolvable small vehicle that carries the nanoparticles deep down in the lung. The microscale carrier will be suited for use with different types of nanoparticles, and the concept of nano-on-microparticle distribution will eliminate the need of coarse carrier. In the present investigation, we have prepared six types of chitosan nanoparticles and one microscale lactose-PEG3000 carrier with volume median diameter of 5 μm (mass median aerodynamic diameter ~2.5 μm). The physicochemical characteristics of nanoparticles namely size, size distribution, zeta potential, roughness, circularity, and crystallinity were determined. The respective mixtures of nanoparticles-lactose-PEG microscale carrier were produced. The aerosolization and inhalation performance of the nanoparticles in each physical mixture was determined. The physicochemical characteristics of nanoparticles that are critical to succeed their deep lung deposition were identified. The study intends to seek fundamental understanding on nanoparticle characteristics essential for pulmonary drug delivery.

Table 1 – Formulation and processing variables in the preparation of chitosan nanoparticles.

Sample	F1	F2	F3	F4	F5	F6
Acetic acid concentration (%, v/v)	0.5	0.5	0.5	0.5	0.5	1
Chitosan grade	LMW	LMW	LMW	LMW	LMW	HMW
Chitosan concentration (%, w/w)	0.1	0.1	0.1	0.1	0.1	0.05
Excipient	–	–	Tween80[a] (0.025%)	Span 80[a] (0.025%)	Ethanol 70%[a] (75%)	–
Solution feeding rate (ml/min)	1.8	3	1.8	1.8	1.8	1.8
Feeding line number	1	2	1	1	1	1
Inlet temperature (°C)	70	70	70	70	70	70
Outlet temperature (°C)	24.9	24.8	24.4	25.2	26.6	26
Atomizing air pressure (bar)	6	6	6	6	6	6

LMW: low molecular weight chitosan; HMW: high molecular weight chitosan.
[a] The liquid surface tension was determined by K-6 surface tensiometer (KRŰSS GmbH Germany) equipped with a wire ring made of a platinum-iridium at 25 ± 1 °C. At least triplicates were carried out for each sample and the results averaged.

2. Materials and methods

2.1. Materials

Low-molecular-weight chitosan (molecular weight: 20 000–50 000 Da, degree of deacetylation ≥ 90%; Zhejiang Aoxing Biotechnology Co. Ltd., China) and high-molecular-weight chitosan (molecular weight: 310 000–375 000 Da, degree of deacetylation ≥ 75.0%; Sigma-Aldrich, Ireland) were used as the matrix material of nanoparticles with glacial acetic acid as the solvent of chitosan (Merck, Germany). Tween 80 (Fisher Scientific, UK), span 80 (Merck, Germany) and ethanol absolute for analysis (Merck, Germany) were used as additives. Lithium acetate anhydrous (ACROS Organics™, USA), ninhydrin and hydrindantin (Sigma-Aldrich, USA) were used in quantification assay of chitosan. Lactose monohydrate (Sorbolac 400; Meggle, Germany) was used as the microparticulate carrier with polyethylene glycol 3000 (PEG3000; Merck, Germany) as the stabilizer.

2.2. Preparation of chitosan nanoparticles

Six different chitosan nanoparticle variants were prepared namely F1, F2, F3, F4, F5, and F6 by spray drying method. The chitosan solutions were first prepared by dissolving the chitosan in acetic acid solution at 25 ± 1 °C under continuous magnetic stirring for 5 h. They were then spray-dried using a nanospray dryer (TwinNanoSpray, UiTM, Malaysia) as a function of variables such as concentration of acetic acid solution, concentration and grade of chitosan, excipients, and processing procedure as summarized in Table 1 [29,30]. The spray drying process was accompanied by atomization of solution into fine droplets followed by hot air evaporation of solvent to produce dried powders. The spray-dried powders were accumulated at the collecting electrode and retrieved using rubber spatula into a 10 ml amber diagnostic vial. The sample was conditioned in a silica gel desiccator and kept at 25 ± 1 °C.

2.3. Preparation of lactose-PEG3000 microparticles

Lactose was added to distilled water, in which 2.5% (w/w) PEG3000 expressed with reference to lactose mass was present, to give a concentration of 2% (w/w) at 25 ± 1 °C. The solution was spray-dried using a nanospray dryer (TwinNanoSpray, UiTM, Malaysia) of which gave rise to the formation of microparticles as a function of the formulation and by means of the following operating parameters: inlet temperature = 70 °C, outlet temperature = 24.5 °C, solution feed rate = 2 ml/min using one feeding line, atomizing air pressure = 5.5 bar. The spray-dried powder was accumulated at the collecting electrode and retrieved using a rubber spatula into a 30 ml clear glass powder jar. The sample was conditioned in a silica gel desiccator and kept at 25 ± 1 °C.

2.4. Physicochemical characterization of chitosan nanoparticles

2.4.1. Size

The size of nanoparticles was determined using the photon correlation spectroscopy by means of a Zetasizer (Nano ZS 90, Malvern Instruments Ltd, UK) at 25 ± 1 °C and a scattering angle of 90°. Five milligram nanoparticles were dispersed in 30 ml deionized water under continuous magnetic stirring prior test. The mean diameter of the nanoparticulate population and its polydispersity index were measured. Means and standard deviations (mean ± SD) were calculated from three determinations.

2.4.2. Zeta potential

The zeta potential of nanoparticles was measured by means of a Zetasizer (Nano ZS 90, Malvern Instruments Ltd, UK) at 25 ± 1 °C. Five milligram nanoparticles were dispersed in 30 ml deionized water under continuous magnetic stirring. The dispersion was loaded in a folded capillary zeta cell for test. Its electrostatic mobility was converted into zeta-potential using the Helmholtz–Smoluchowski equation [31]. Mean ± SD were calculated from three measurements.

2.4.3. Scanning electron microscopy

Scanning electron microscopy (SEM) technique was used to examine the surface morphology of nanoparticles. The images of particles were taken by using Quanta 450 FEG scanning electron microscope (FEI, Netherlands). The sample was first adhered onto a carbon tape and then sputter-coated by platinum (JFC-1600 Auto Fine Coater, JEOL, Japan) with a thickness of 5 nm. The surface roughness and circularity of nanoparticles were analyzed with image processing software ImageJ (NiH, USA). The original SEM image was first converted to grey-scale (8-bit) image and subsequently to binary image. The plugin "Analyze Particle" and 'Roughness Calculation" were run to measure the circularity and roughness. Mean ± SD of arithmetic mean roughness (R_a) and circularity (Circ) were calculated from nine measurements of three images.

2.4.4. X-ray powder diffraction (XRPD)

The crystallinity of nanoparticles was determined using the X-ray diffractometer (Ultima IV, Rigaku Coperation, Japan) with diffraction angle (2θ) ranging from 3° to 60° and a scanning speed of 5°/min. Cu–Kα radiation was used as the x-ray resource at 40 kV and 30 mA. Mean ± SD were calculated from three measurements. The chitosan crystallinity index (cCI; %) was determined using the following equation:

$$\text{cCI\%} = \frac{(I_{110} - I_{\text{amor}}) \times 100}{I_{110}} \quad (1)$$

where I_{110} is the maximum intensity at 20° and I_{amor} is the intensity of amorphous diffraction at 16° [32,33].

2.5. Physicochemical characterization of lactose-PEG3000 microparticles

The SEM and XRPD techniques were similarly adopted to assess the surface morphology and crystallinity of lactose-PEG3000 microparticles. Other characterizations such as density and size were conducted.

2.5.1. Density

Bulk and tapped density were measured by using a 5 ml measuring cylinder. The cylinder was filled with a known weight of powder and the bulk volume was recorded. The cylinder was tapped 200 times, where no further reduction in powder bed volume, at a rate of 4 times per second and the new volume was recorded (tapped volume). The bulk density (ρb) and tapped density (ρt) were calculated, and mean ± SD were determined from three measurements.

Carr's index and Hausner ratio were derived from the bulk density and tapped density values of powder using the following equations:

$$\text{Carr's index (\%)} = (1 - \rho b/\rho t) \times 100\% \quad (2)$$

$$\text{Hausner ratio} = \rho t/\rho b \quad (3)$$

2.5.2. Size

Lactose-PEG3000 microparticle size distribution was determined using the laser diffraction method (Mastersizer 2000, Malvern Instruments Ltd, UK) equipped with a Scirocco 2000 dry powder dispersing system operated at a pressure of 1 bar. The particle size distribution was characterized by the volume median diameter d_{50}, d_{10} and d_{90} values corresponding to 50%, 10% and 90% of microparticles with size lying below the specified diameter. Measurement was run in triplicate and results averaged.

2.6. In vitro aerosolization and inhalation performance

The Andersen Cascade Impactor (ACI; Copley Scientific Ltd, UK) was used according to the compendial procedures [34]. All parts of the ACI were first washed with deionized water and allowed to dry. Then the ACI was assembled from stage F up to stage 0. A Glass fiber filter (Copley Scientific Ltd, UK) was inserted after stage 7 to collect small particles that might escape from the stage 7. The stages were clamped together and sealed with FDA approved silicone rubber O-rings in order to prevent inter-stage leak. A pre-separator was fixed onto stage 0 and connected to an induction port. The induction port was connected into a mouthpiece adapter to provide an airtight seal between the induction port and the Handihaler® device (Boehringer Ingelheim, Germany). ACI was connected to a vacuum source (Low Capacity Pumps Models LCP5, Copley Scientific Ltd, UK) through a critical flow controller (TPK 2000, Copley Scientific Ltd, UK). The connection was made via vacuum PVC tubing (10 mm internal diameter).

The chitosan nanoparticles and lactose-PEG3000 microparticles were mixed at a weight ratio of 1:9 through vortex-blending at 40 Hz for 30 min (VelpScientifica, Italy). A size-2 capsule (Capsules halal clear, San Tronic Medical Devices, Malaysia) was packed with 30 mg of the premixed nano/micro powder. The capsule was placed in the centre chamber of a breath-activated dry powder inhaler device. The powder was actuated to anderson cascade impactor via inhaler under an air flow rate of 48 l/min for 5 s corresponding to a pressure drop of 4 kPa which represented the normal pressure drop in human lung. Cut-off diameter of each stage was recalculated at a flow rate 48 l/min according to Eq. (4) and was as follows: Stage 0, 6.91 µm; Stage 1, 4.45 µm; Stage 2, 3.61 µm; Stage 3, 2.53 µm; Stage 4, 1.61 µm; Stage 5, 0.84 µm; Stage 6, 0.54 µm; and Stage 7, 0.31 µm.

$$D_{50,48} = D_{50,28.3}\left(\frac{28.3}{48}\right)^{\frac{1}{2}} \quad (4)$$

where $D_{50,48}$ and $D_{50,28.3}$ are the cut-off diameter of a stage at flow rate 48 and 28.3 l/min, respectively.

Five capsules were emptied, one in each run. The powder emitted from each capsule was deposited on ACI stages. Then ACI apparatus was dismantled. The powder was carefully collected by using 0.5% (v/v) acetic acid solution from mouthpiece, induction port, pre-separator, the inner walls and collection plate of each stage, and filter into separate glass scintillation vials. Vials were shaken at 25 ± 1 °C for 5 h in a shaker bath (ST402, Nuve, Turkey) before quantifying for chitosan. The respective chitosan content was then assessed using the ninhydrin assay method [35]. Samples were subjected to spectrophotometric assay using UV-VIS spectrophotometer (Cary 50 Conc, Varian Australia

Pty. Ltd., Australia) at a wavelength maximal of 570 nm for chitosan. The limit of detection is 0.048 mg/ml. The limit of quantification is 0.160 mg/ml. Linearity ranges are 0.025–1.000 mg/ml. Triplicates were conducted and the results averaged.

The emitted dose (ED) was determined as the sum of chitosan mass collected from mouthpiece, induction port, pre-separator, and all stages. Deposited dose (DD) is the sum of chitosan mass deposited on stages 0 to F. Percent dispersed (PD) was used to express the percentage of ED based on the total dose (TD) using Eq. (5). Percent inhaled (PI) was used to express the percentage of DD based on the TD using Eq. (6). The fine particle doses (FPD) were calculated at three levels namely, $FPD_{<4.5\ \mu m}$, $FPD_{<3.6\ \mu m}$, and $_{0.5\ \mu m<}FPD_{<3.6\ \mu m}$ as the dose deposited on stages 2 to F, stages 3 to F, and stages 3–7, respectively. The first level exhibited particles deposited on deep lung generally. Second level represented particles deposited on peripheral lung. Second level with particles prone to be exhaled (<500 nm) excluded was presented as level three.

The fine particle fraction (FPF) was expressed as the percentage of FPD to ED using Eq. (7). The respirable fraction (RF) was expressed as the percentage of FPD to the DD using Eq. (8).

$$\text{Percent dispersed (PD)\%} = \frac{\text{ED}}{\text{TD}} \times 100 \quad (5)$$

$$\text{Percent inhaled (PI)\%} = \frac{\text{DD}}{\text{TD}} \times 100 \quad (6)$$

$$\text{Fine particle fraction (FPF)\%} = \frac{\text{FPD}}{\text{ED}} \times 100 \quad (7)$$

$$\text{Respirable fraction (RF)} = \frac{\text{FPD}}{\text{DD}} \times 100 \quad (8)$$

The cumulative particle size distribution functions obtained from the ACI was plotted on log probability graph. The mass median aerodynamic diameter (MMAD) was calculated as the particle size at the 50th percentile on the graph. The geometric standard deviation (GSD) was calculated as the square root of the ratio of particle size at the 84.13th percentile to the 15.87th percentile. All aerosolization and inhalation parameters were expressed in means and standard deviations obtained from triplicates of experiments.

2.7. Fourier transform infrared (FTIR) spectroscopy

F2 and F4 powders collected from stages 0–7 were analyzed by FTIR spectrometer (Spectrum 100, PerkinElmer, USA) over a scanning range between 400 and 4000 cm^{-1} at a resolution of 4 cm^{-1}. The powder sample was blended with potassium bromide at 1:99 weight ratio and ground into fine powder. This mixture was then transferred into a pellet die (diameter 13 mm), which was placed inside a 15 ton hydraulic pellet press (Specac Ltd., UK). An axial load was applied and increased slowly to a value of 10 tons, and held at a constant pressure for 2 min. The formed thin disc was subjected to FTIR spectroscopy analysis following the aforementioned treatment. Three reference powders namely chitosan nanoparticles, lactose-PEG3000 microparticles and their mixture at a weight ratio of 1:9 were similarly characterized. The absorbance spectra of powder samples from ACI tests were compared and correlated against the reference samples using PerkinElmer Spectrum Version 10.3.6 software (PerkinElmer Inc, USA). All correlations were expressed in mean ± SD from triplicates of experiment. The correlation coefficient was calculated using the following equation [36]:

$$\text{Correlation coefficient} = \frac{\sum w_i A_i B_i}{(\sum w_i A_i A_i)^{0.5} \times (\sum w_i B_i B_i)^{0.5}} \quad (9)$$

where A_i and B_i were the absorbance values in spectra of test powder and reference powder at frequency i, and w_i is a statistical weighting factor.

2.8. Statistical analysis

Results were expressed as a mean of at least three experiments with the corresponding standard deviation. Pearson correlation was carried out using SPSS software 18.0 when applicable. A statistically significance was denoted by $P < 0.05$ unless otherwise stated.

3. Results and discussion

3.1. Chitosan nanoparticles

Six chitosan nanoparticle variants were produced in accordance to the formulation and processing parameters outlined in Table 1. Table 2 summarizes the physicochemical attributes of these chitosan nanoparticles.

3.1.1. Size

The nanoparticle variants were characterized by sizes ranged between 275.67 ± 15.22 nm (F3) and 684.00 ± 17.61 nm (F2) (Table 2). With reference to F2 and F1, an increase in nanoparticle size was observed with the use of two liquid feeding lines during the course of nanospray drying. Double feeding lines increased the amount of chitosan solution entering the nozzle at a time thus rendering the formation of larger droplets and nanoparticles thereafter.

A reduction in surface tension of liquid droplets tends to be accompanied by reduced droplet and particle sizes [37]. Using the hydrophilic surfactant (Tween 80) in F3, it was anticipated that the liquid droplets' surface tension was reduced (0.5% acetic acid solution = 73 ± 5 mN/m; 0.025% tween 80 solution = 46 ± 1 mN/m). Small liquid droplets were formed during the atomization step and small solid nanoparticles were thereby collected (Table 2). A more hydrophobic surfactant (Span 80) was used in F4. Span 80 brought about reduced surface tension and helped to produce small liquid droplets and solid nanoparticles as in the case of Tween 80 (0.025% Span 80 solution = 35 ± 1 mN/m), though not as small as those in F3 (Table 2).

The nanoparticle size was also reducible by dissolving the chitosan in ethanol-water mixture prior spray drying (F5) (Table 2). Ethanol is a popular polar solvent which acts as a surface active agent (31 ± 1 mN/m) [38]. Using ethanol, the surface tension of liquid droplets decreased. Small liquid

Table 2 – Physicochemical characteristics of chitosan nanoparticles and lactose-PEG3000 microparticles.

(a) Physicochemical characteristics of chitosan nanoparticles

	F1	F2	F3	F4	F5	F6
Z-average size (nm)	610.03 ± 29.97	684.00 ± 17.61	275.67 ± 15.22	465.17 ± 58.74	338.70 ± 7.50	347.27 ± 19.39
Zeta potential (mV)	27.47 ± 1.87	27.86 ± 1.27	13.60 ± 2.36	13.10 ± 1.49	14.47 ± 0.23	20.17 ± 2.62
Polydispersity index	0.63 ± 0.12	0.57 ± 0.01	0.58 ± 0.01	0.80± 0.21	0.81 ± 0.12	0.42 ± 0.05
Circularity	0.90 ± 0.21	0.90 ± 0.23	0.82 ± 0.28	0.82 ± 0.26	0.87 ± 0.23	0.88 ± 0.23
Roughness (nm)	0.208 ± 0.004	0.379 ± 0.008	0.249 ± 0.004	0.301 ± 0.001	0.184 ± 0.003	0.211 ± 0.001
Crystallinity (%)	24.71 ± 1.85	19.40 ± 2.23	25.34 ± 0.69	27.02 ± 1.59	18.56 ± 1.01	18.72 ± 2.12

(b) Physicochemical characteristics of lactose-PEG3000 microparticles

d_{10} (μm)	1.58 ± 0.01	Circularity	0.16 ± 0.06	Tapped density (g/cm^3)	0.2125 ± 0.0038
d_{50} (μm)	5.43 ± 0.10	Roughness (nm)	127.21 ± 1.11	Carr's index (%)	51.91 ± 0.13
d_{90} (μm)	54.60 ± 1.7	Bulk density (g/cm^3)	0.1022 ± 0.0018	Hausner ratio	2.08 ± 0.01

droplets and solid nanoparticles with sizes ranging between F3 and F4 were obtainable.

High molecular weight chitosan was used in F6 preparation. Unexpectedly, the nanoparticle size of F6 was small (Table 2). This might be due to two reasons. First, the chitosan was used at a lower concentration of 0.05% instead of 0.1% (w/w). Second, the high molecular weight chitosan has long chains which were able to entangle between each other into more compacted particles than those of F1 and F2. Earlier study by Mohd Chachuli et al. [39] indicated that the lower molecular weight chitosan might not be translated to smaller nanoparticles due to reduced chain entanglement tendency. The F6 also demonstrated a relatively low polydispersity index (Table 2), when compared to nanoparticles prepared from other formulation and processing conditions. Apparently, the entangled chains of high molecular weight chitosan in a diluted liquid medium could translate to less risks of chain disentanglement, and formation of populations with diverse sizes.

3.1.2. *Zeta potential*

Chitosan nanoparticles of F3, F4, and F5 were characterized by lower zeta potential values than F1 and F2 (Table 2). The reduction in the surface charge of the nanoparticles was attributed to the non-ionic surfactant molecules decorated onto the surfaces of nanoparticles and/or reorientation of chitosan chains in nanomatrices due to the surrounding organic solvent in the course of spray drying which could take place following polymer-additive interaction [40]. Using high molecular weight chitosan in F6, the nanoparticulate surface charges were similarly reduced. Such observation was also noted in the study of Kouchak et al. [41]. The reduction in zeta potential of solid nanoparticles prepared from high molecular weight chitosan might be an attribute of reduced degree of deacetylation when compared to that of low molecular weight chitosan.

3.1.3. *Morphology*

Fig. 1 shows the typical morphology of nanoparticles. Nanoparticles of all formulations were spherical in shape with some variations. F1 and F2 had the most uniform spherical shape with circularity values of 0.90 ± 0.21 and 0.90 ± 0.23, respectively (Table 2). F3 and F4 had the lowest circularity values of 0.82 ± 0.28 and 0.82 ± 0.26, respectively.

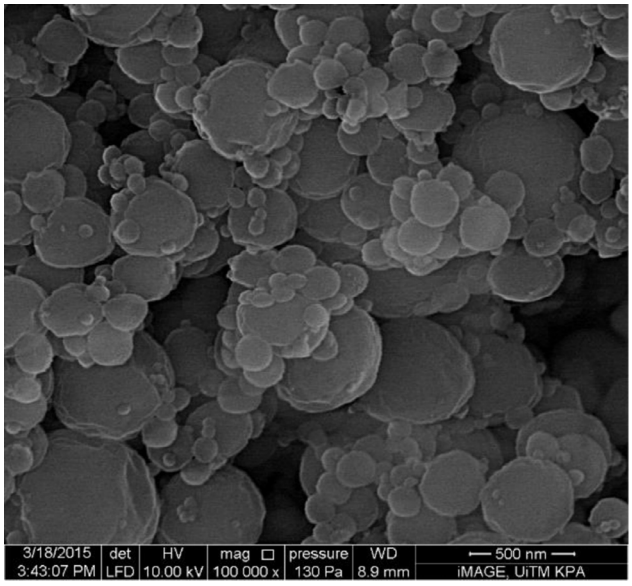

Fig. 1 – Scanning electron microscopic images of spray-dried chitosan nanoparticles.

3.1.4. *Crystallinity*

Overall, the crystallinity of F1 to F6 nanoparticles was lower than chitosan (cCI = 51.65% ± 1.49%) (Table 2; Fig. 2). Among all formulations, low molecular weight chitosan nanoparticles formulated with span 80 and tween 80 exhibited a relatively high level of matrix crystallinity (Table 2). The short chains of chitosan, in the presence of surfactants, appeared to be able to rearrange into a more systematic domain during the process of spray drying.

3.2. *Lactose-PEG3000 microparticles*

The lactose-PEG3000 microparticles were characterized by a non-spherical shape with a circularity value of 0.16 ± 0.06,

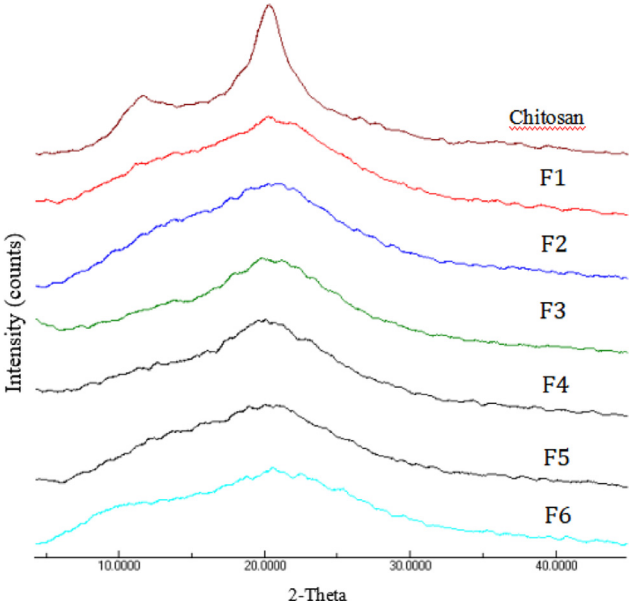

Fig. 2 – X-ray powder diffractograms of chitosan and chitosan nanoparticles.

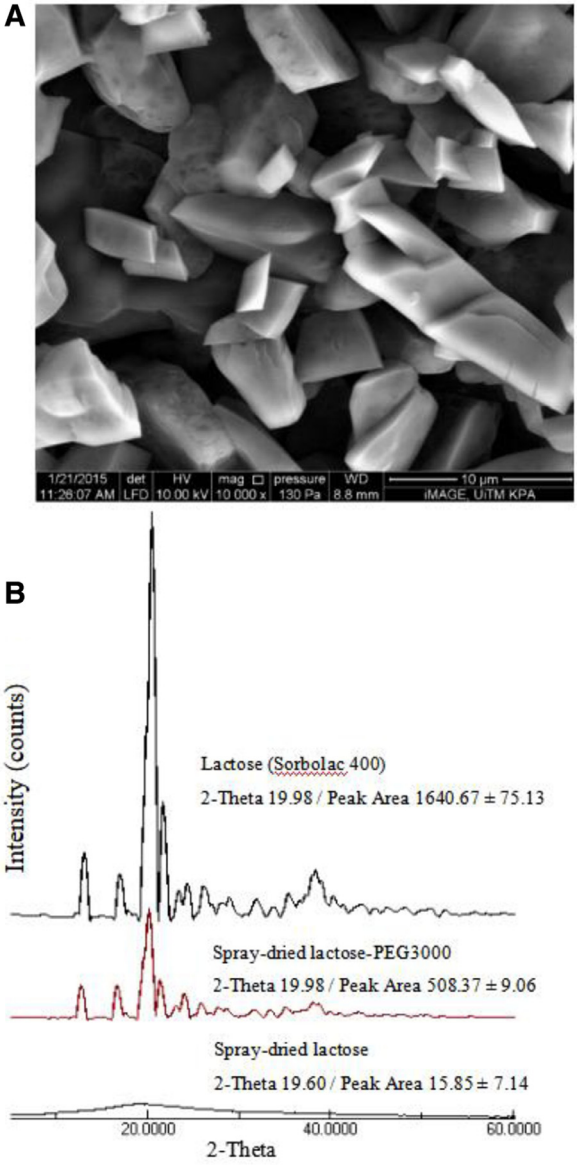

Fig. 3 – (A) Scanning electron microscopic image of spray-dried lactose-PEG3000 microparticles. (B) X-ray powder diffractograms of unprocessed lactose, spray-dried lactose, and spray-dried lactose-PEG3000 microparticles.

unlike lactose particles as reported by Majid and Wong [42] due to the presence of PEG3000 (Fig. 3A; Table 2). They were characterized by a surface roughness R_a of 127.21 ± 1.11 nm (Fig. 3A; Table 2). Lactose-PEG3000 powder had d_{10}, d_{50} and d_{90} of 1.58 ± 0.01, 5.43 ± 0.10 and 54.60 ± 1.7 µm, respectively. Lactose-PEG3000 powder bulk and tapped density were 0.1022 ± 0.0018 and 0.2125 ± 0.0038 g/cm^3, respectively. Their Carr's index and Hausner ratio were 51.91% ± 0.13% and 2.08 ± 0.01, respectively.

The lactose microparticles, being small in dimension, have been met with hygroscopic issues. PEG3000 was reported to be able to convert the lactose into a more crystalline matrix [43,44] thereby reducing lactose hygroscopicity via its affinity to form hydrogen bonds with water during spray drying process and slow down the lactose drying rate. Analysis of XRD patterns for lactose before and after spray drying with and without PEG3000 indicated that the spray-dried lactose without PEG3000 underwent a great reduction in magnitude of XRD peaks compared with spray-dried lactose-PEG3000 microparticles (Fig. 3B). The level of crystallinity of lactose-PEG3000 microparticles was higher than that of spray-dried lactose without the PEG3000 (Fig. 3B). The α-lactose monohydrate had its primary XRD peak at $2\theta = 19.98°$. A tremendous decrease in peak areas from unprocessed lactose toward spray-dried lactose without PEG3000 was observed with peak slightly shifted from 19.98° to 19.60° (Fig. 3B). A less drastic change was, however, noted in the case of lactose-PEG3000 microparticles.

3.3. *Aerosolization and inhalation performance of chitosan nanoparticles*

Six chitosan nanoparticles/lactose-PEG3000 microparticles mixtures in the weight ratio of 1:9 were prepared and subjected to cascade impaction analysis. The fine particles and respirable fractions were taken at three particle size levels namely particles with MMAD less than 4.5 µm, less than 3.6 µm and between 3.6 and 0.5 µm. The first level represented particles suitable for deep lung deposition. The second level exhibited particles with the best aerodynamic diameter for peripheral lung delivery. Excluding particles with diameter less than 0.5 µm, which are prone to be exhaled from the second level, was represented by level three.

All formulations were well dispersed and emitted from the inhaler device (Table 3) in comparison to chitosan nanoparticles tested without blending with lactose-PEG3000 microparticles (F2 only: PD = 58.12% ± 23.30%; PI = 27.27% ± 12.62%). F3 had the lowest emitted dose

Table 3 – Aerosolization and inhalation profiles of chitosan nanoparticles in lactose-PEG3000 microparticles.

	F1	F2	F3	F4	F5	F6
MMAD (μm)	4.13 ± 0.59	4.25 ± 0.85	4.40 ± 0.85	4.70 ± 0.16	7.65 ± 0.90	3.85 ± 0.47
GSD	4.27 ± 1.41	5.14 ± 0.35	1.76 ± 0.12	2.11 ± 0.65	4.23 ± 0.47	3.71 ± 0.95
TD (mg)	15	15	15	15	15	15
ED (mg)	12.34 ± 1.18	12.41 ± 1.79	10.11 ± 1.69	12.81 ± 0.84	12.33 ± 1.97	11.78 ± 0.37
DD (mg)	5.46 ± 0.93	6.66 ± 1.33	4,38 ± 0.58	4.45 ± 1.25	5.85 ± 1.10	4.84 ± 0.59
PD (%)	82.29 ± 7.87	82.74 ± 11.99	67.45 ± 11.29	85.37 ± 5.64	82.18 ± 13.11	78.52 ± 2.47
PI (%)	36.42 ± 6.22	44.43 ± 8.84	29.22 ± 3.88	29.69 ± 8.39	38.98 ± 7.36	32.29 ± 3.95
Particles < 4.5 μm						
FPD (mg)	3.82 ± 0.72	4.63 ± 1.16	2.81 ± 0.69	2.71 ± 0.99	3.40 ± 0.87	3.82 ± 0.32
FPF (%)	30.83 ± 3.89	36.96 ± 4.64	27.54 ± 2.48	20.92 ± 6.69	27.31 ± 3.01	32.42 ± 2.07
RF (%)	69.79 ± 1.24	69.01 ± 3.98	63.45 ± 7.47	59.98 ± 7.15	57.69 ± 5.19	79.14 ± 3.17
Particles < 3.6 μm						
FPD (mg)	1.98 ± 0.39	2.78 ± 0.85	1.12 ± 0.45	1.16 ± 0.54	1.29 ± 0.34	1.70 ± 0.28
FPF (%)	15.94 ± 1.63	22.15 ± 4.25	10.90 ± 3.02	9.04 ± 3.91	10.31 ± 1.24	14.33 ± 2.05
RF (%)	36.26 ± 3.37	41.23 ± 5.05	25.01 ± 6.94	26.68 ± 10.07	21.76 ± 2.01	34.80 ± 1.50
0.5 μm < Particles < 3.6 μm						
FPD (mg)	1.38 ± 0.68	1.98 ± 0.61	0.99 ± 0.42	1.04 ± 0.47	1.07 ± 0.24	1.17 ± 0.56
FPF (%)	12.93 ± 4.39	15.75 ± 3.08	9.73 ± 3.25	8.09 ± 3.49	9.59 ± 0.66	10.92 ± 4.59
RF (%)	26.99 ± 9.83	29.31 ± 3.70	22.25 ± 7.13	24.25 ± 10.57	19.16 ± 1.08	25.77 ± 9.17

Table 4 – Relationship of fine particle fraction of chitosan nanoparticles with their physicochemical characteristics.

	$FPF_{<4.5}$		$FPF_{<3.6}$		$_{0.5<}FPF_{<3.6}$	
	r	*p*	*r*	*p*	*r*	*p*
Z-average size	0.475	0.341	0.770[a]	0.073	0.778[a]	0.068
Zeta potential	0.817[b]	0.047	0.916[b]	0.010	0.932[b]	0.007
Polydispersity index	−0.692	0.127	−0.527	0.283	−0.465	0.353
Roughness	0.262	0.616	0.547	0.261	0.481	0.627
Circularity	0.815[b]	0.048	0.788[a]	0.062	0.815[b]	0.048
Crystallinity	−0.648	0.164	−0.425	0.401	−0.402	0.430

Correlation is significant at [a]0.10 level, [b]0.05 level.

and percent dispersibility. This can be ascribed to strong attachment force between the powder particles and the wall of the gelatin capsule as a result of binding affinity of tween 80 available on the surfaces of nanoparticles. Generally, F1 and F2 exhibited higher DD, PD, PI, FPD, FPF and RF, whereas F3 and F4 provided the otherwise aerosolization and inhalation performances.

FPF at all levels was strongly correlated with nanoparticle surface charges (Table 4). The higher the surface charges of nanoparticles, the tendency of them to agglomerate was lower. More nanoparticles can then be attached onto the lactose-PEG3000 microparticles and available for lung deposition at lower stages. Fig. 4 demonstrated the morphological images of chitosan nanoparticles interacting with lactose-PEG3000 microparticles (Supp. 1 with lower magnification). With reference to F3 and F4, these nanoparticles tend to cluster around the lactose-PEG3000 microparticles instead of spreading over the microparticulate surfaces. They were less free flow and this could be due to reduced surface charges and inter-particulate repulsion as well as additional binding affinity conferred by tween 80 and span 80 that were available on the nanoparticles' surfaces. Overall, the chitosan nanoparticles (F1–F6) were adhered on the surfaces of lactose-PEG3000 microparticles. The adherence of chitosan nanoparticles formulated with span 80 appeared weak (Fig. 4). This was likely due to hydrophilicity-hydrophobicity mismatch between the hydrophobic surfactant and polar lactose-PEG3000 presented at the interface of nanoparticles and microparticles.

Spherical nanoparticles had the lowest specific surface area for attachment onto other surfaces. Decreasing the shape uniformity of a sphere led to more areas of one surface that can be attached to another surfaces. Increasing the attachment surface area between carrier and nanoparticles or between nanoparticles will increase the attachment force between them. In the present study, the less spherical nanoparticles brought about lower FPFs (Table 4). The inter-nanoparticle attachment could negate the attachment of nanoparticles onto the surfaces of lactose-PEG3000 microparticles. This could then reduce the availability of nanoparticles for deposition at the lower lung regions. The inter-nanoparticle attachment was expected to proceed at a greater propensity than nanoparticles-microparticles attachment. This was aptly explained by the latter involving lactose-PEG3000 matrices which were larger in size and had a lower specific surface area to interact with the surrounding nanoparticles. Under the influence of nanoparticle shape,

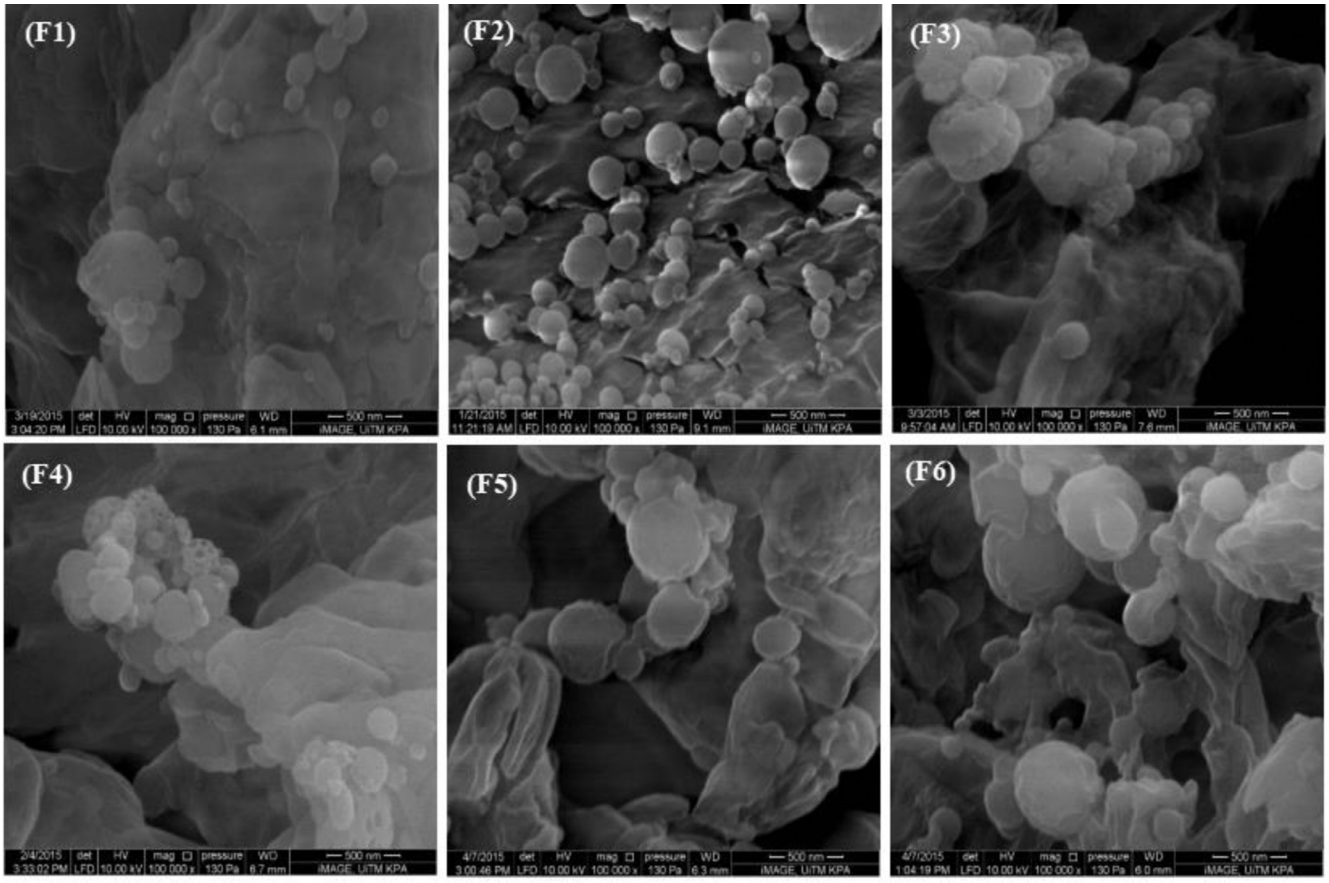

Fig. 4 – Scanning electron microscopic images of spray-dried chitosan nanoparticles/lactose-PEG3000 microparticles mixtures.

the attachment affinity between nanoparticles exerted a predominating effect on FPF over the attachment tendency between the nanoparticles and microparticles.

The size of nanoparticles brought about similar influences on FPF as in the case of their shape and zeta potential attributes (Table 4), where larger nanoparticles were deemed to exhibit a smaller specific surface area with reduced inclination of inter-nanoparticulate attachment. The larger nanoparticles were largely interacted with the lactose PEG3000 microparticles and aided by them to reach the lower lung regions.

Carrier particle crystallinity is known to affect the aerosolization and pulmonary inhalation profiles of adsorbates. The creation of highly crystalline carrier particles with lower surface energy is envisaged to facilitate pulmonary adsorbate deposition [45]. The influences of adsorbate crystallinity on pulmonary inhalation however has yet to be studied. The present investigation indicated that the crystallinity profiles of chitosan nanoparticles (adsorbate) had no significant bearing on the fine particle fraction (Table 4).

3.4. *FTIR study*

Nanoparticles' shape and zeta potential exerted the strongest influences on their lung deposition manner (Table 4). Among all batches of nanoparticles, F2 were characterized by the highest circularity and positive zeta potential values whereas F4 had the lowest values. Both F2 and F4 were selected in examination of attachment/detachment manner of chitosan nanoparticles against the lactose-PEG3000 microparticles during the processes of aerosolization and inhalation using the FTIR spectra correlation approach (Supp. 2).

The correlation between the FTIR spectra of the collected powder of F2 or F4 at each stage of cascade impactor and the reference powder did not necessarily reflect the amount of its components. The correlation instead reflected the changes in the component ratio of the powder. A marked change in the spectra correlation took place after stage 3 in F2 where the powder collected in stage 4 and thereafter possessed stronger characteristics of chitosan nanopaticles with reduced features of lactose-PEG3000 microparticles (Table 5). The stage 3 had a cut-off diameter of 2.53 μm while the MMAD of the microcarrier was 2.50 μm. The powders collected from stages subsequent to stage 3 were anticipated to show a reduction in the lactose-PEG3000 microparticles to chitosan nanoparticles weight ratio (Table 5).

With reference to F2, the spectra of powder collected at stage 0–3 were highly correlated to the spectra of the original powder mixture and lactose-PEG3000 microparticles of which represented to main component in the mixture. The chitosan nanoparticles were attached to lactose-PEG3000 particles and deposited together at stages 0–3. Powders at stages 4, 5

Table 5 – FTIR spectra correlation values of F2 and F4 against chitosan nanoparticles, lactose-PEG3000 microparticles and their mixture (1.000 denotes 100% correlation).

Stage	F2			F4		
	Chitosan nanoparticles	Lactose-PEG3000 microparticles	Mixture	Chitosan nanoparticles	Lactose-PEG3000 microparticles	Mixture
0	0.532 ± 0.013	0.982 ± 0.007	0.989 ± 0.005	0.564 ± 0.027	0.896 ± 0.020	0.993 ± 0.003
1	0.534 ± 0.009	0.958 ± 0.006	0.984 ± 0.007	0.442 ± 0.053	0.838 ± 0.009	0.882 ± 0.029
2	0.528 ± 0.008	0.948 ± 0.008	0.988 ± 0.004	0.424 ± 0.047	0.871 ± 0.059	0.768 ± 0.066
3	0.576 ± 0.010	0.955 ± 0.003	0.983 ± 0.001	0.418 ± 0.042	0.811 ± 0.058	0.711 ± 0.060
4	0.701 ± 0.046	0.841 ± 0.031	0.823 ± 0.030	0.477 ± 0.049	0.765 ± 0.047	0.822 ± 0.067
5	0.709 ± 0.012	0.911 ± 0.001	0.886 ± 0.004	0.653 ± 0.028	0.805 ± 0.019	0.935 ± 0.021
6	0.653 ± 0.007	0.919 ± 0.004	0.893 ± 0.005	0.177 ± 0.038	0.363 ± 0.060	0.424 ± 0.075
7	0.928 ± 0.005	0.497 ± 0.010	0.555 ± 0.011	0.069 ± 0.096	0.047 ± 0.068	0.051 ± 0.068

and 6 seemed to have different weight ratios of chitosan nanoparticles to lactose-PEG3000 microparticles from those at stages 0–3. Spectra correlation analysis indicated that an increase in weight ratio of chitosan nanoparticles in relation to lactose-PEG3000 microparticles took place after the first filter point of stage 3. At stage 7, chitosan nanoparticles became the predominant component in the collected powder. A sharp drop in the lactose-PEG3000 microparticle fraction was noted in powder collected at stage 7. Similar observations were however not found in the case of F4. This was probably due to loss of surfactant from the chitosan nanoparticles onto the impactor surfaces at lower stages that rendered the FTIR characteristics of nanoparticles altered and less detectable.

Chitosan nanoparticles, apart from having their aerosolization and inhalation facilitated by lactose-PEG3000 microparticles as highlighted in Section 3.3, their addition into lactose-PEG3000 microparticles had also improved the flow properties of the latter (Table 2b; Chitosan nanoparticles F2/lactose-PEG3000 microparticles mix: Hausner ratio = 1.56 ± 0.13; Carr's index = 35.61% ± 5.19%).

4. Conclusions

The chitosan nanoparticles, physically mixed with fine lactose-PEG3000 microparticles, exhibit a comparable inhalation performance with the commercially available dry powder inhaler products where the FPF lies between 20% and 30% [46]. Both aerosolization and inhalation performances of chitosan nanoparticles are primarily governed by their zeta potential, circularity and size. Chitosan nanoparticles characterized by a larger magnitude of zeta potential, higher levels of circularity and sizes are envisaged to undergo a lower extent of inter-nanoparticulate aggregation, and have largely interacted with fine lactose-PEG3000 microparticles that aid their delivery to the lower lung regions. The present fundamental findings can serve as a guide to nanoparticle design and help to explain the pulmonary delivery outcomes of the drug in the future developments.

Conflicts of interest

The authors declare that there is no conflicts of interest.

Acknowledgments

The authors wish to thank Universiti Teknologi MARA, and Ministry of Higher Education of Malaysia for fund (0141903), LRGS-NanoMITe RU029-2014 and facility support.

Supplementary materials

Supplementary material associated with this article can be found, in the online version, at doi:10.1016/j.ajps.2019.02.001.

REFERENCES

[1] Bailey MM, Berkland CJ. Nanoparticle formulations in pulmonary drug delivery. Med Res Rev 2009;29:196–212.
[2] Sun T, Zhang YS, Pang B, Hyun DC, Yang M, Xia Y. Engineered nanoparticles for drug delivery in cancer therapy. Angew Chem Int Ed 2014;53(46):12320–64.
[3] Sundar S, Prajapati VK. Drug targeting to infectious diseases by nanoparticles surface functionalized with special biomolecules. Curr Med Chem 2012;19:3196–202.
[4] Khadka P, Ro J, Kim H, Kim I, Kim JT, Kim H, et al. Pharmaceutical particle technologies: an approach to improve drug solubility, dissolution and bioavailability. Asian J Pharm Sci 2014;9(6):304–16.
[5] Peer D, Karp JM, Hong S, Farokhzad OC, Margalit R, Langer R. Nanocarriers as an emerging platform for cancer therapy. Nat Nanotechnol 2007;2(12):751–60.
[6] Liu M, Zhang J, Shan W, Huang Y. Developments of mucus penetrating nanoparticles. Asian J Pharm Sci 2015;10(4):275–82.
[7] Rogueda PGA, Traini D. The nanoscale in pulmonary delivery. Part 1: deposition, fate, toxicology and effects. Exp Opin Drug Deliv 2007;4:595–606.
[8] Pfützner A, Forst T. Pulmonary insulin delivery by means of the Technosphere™ drug carrier mechanism. Exp Opin Drug Deliv 2005;2:1097–106.
[9] Vij N. Nano-based theranostics for chronic obstructive lung diseases: challenges and therapeutic potential. Exp Opin Drug Deliv 2011;8:1105–9.
[10] Yang W, Peters JI, Williams RO III. Inhaled nanoparticles – a current review. Int J Pharm 2008;356:239–47.
[11] Kawakami K, Sumitani C, Yoshihashi Y, Yonemochi E, Terada K. Investigation of the dynamic process during

spray-drying to improve aerodynamic performance of inhalation particles. Int J Pharm 2010;390(2):250–9.
[12] Tsapis N, Bennett D, Jackson B, Weitz DA, Edwards DA. Trojan particles: large porous carriers of nanoparticles for drug delivery. Proc Natl Acad Sci 2002;99(19):12001–5.
[13] Jensen DMK, Cun D, Maltesen MJ, Frokjaer S, Nielsen HM, Foged C. Spray drying of siRNA-containing PLGA nanoparticles intended for inhalation. J Control Rel 2010;142(1):138–45.
[14] Tomoda K, Ohkoshi T, Nakajima T, Makino K. Preparation and properties of inhalable nanocomposite particles: effects of the size, weight ratio of the primary nanoparticles in nanocomposite particles and temperature at a spray-dryer inlet upon properties of nanocomposite particles. Coll Surf B Biointerf 2008;64(1):70–6.
[15] Kho K, Cheow WS, Lie RH, Hadinoto K. Aqueous re-dispersibility of spray-dried antibiotic-loaded polycaprolactone nanoparticle aggregates for inhaled anti-biofilm therapy. Powder Technol 2010;203(3):432–9.
[16] Lebhardt T, Roesler S, Uusitalo HP, Kissel T. Surfactant-free redispersible nanoparticles in fast-dissolving composite microcarriers for dry-powder inhalation. Eur J Pharm Biopharm 2011;78(1):90–6.
[17] Grenha A, Seijo B, Remuñán-López C. Microencapsulated chitosan nanoparticles for lung protein delivery. Eur J Pharm Sci 2005;25:427–37.
[18] Grenha A, Seijo B, Serra C, Remunan-Lopez C. Chitosan nanoparticle-loaded mannitol microspheres: structure and surface characterization. Biomacromol 2007;8(7):2072–9.
[19] Kaye RS, Purewal TS, Alpar HO. Simultaneously manufactured nano-in-micro (SIMANIM) particles for dry-powder modified-release delivery of antibodies. J Pharm Sci 2009;98:4055–68.
[20] Li X, Guo Q, Zheng X, Kong X, Shi S, Chen L, et al. Preparation of honokiol-loaded chitosan microparticles via spray-drying method intended for pulmonary delivery. Drug Deliv 2009;16(3):160–6.
[21] Ohashi K, Kabasawa T, Ozeki T, Okada H. One-step preparation of rifampicin/poly(lactic-co-glycolic acid) nanoparticle-containing mannitol microspheres using a four-fluid nozzle spray drier for inhalation therapy of tuberculosis. J Control Rel 2009;135(1):19–24.
[22] Sham JO, Zhang Y, Finlay WH, Roa WH, Lobenberg R. Formulation and characterization of spray-dried powders containing nanoparticles for aerosol delivery to the lung. Int J Pharm 2004;269(2):457–67.
[23] Ely L, Roa W, Finlay WH, Lobenberg R. Effervescent dry powder for respiratory drug delivery. Eur J Pharm Biopharm 2007;65(3):346–53.
[24] Noraizaan AN, Wong TW. Physicochemical effects of lactose microcarrier on inhalation performance of rifampicin in polymeric nanoparticles. Powder Technol 2017;310:272–81.
[25] Schiffter H, Condliffe J, Vonhoff S. Spray-freeze-drying of nanosuspensions: the manufacture of insulin particles for needle-free ballistic powder delivery. J R Soc Interf 2010;7:S483–500.
[26] Abdelwahed W, Degobert G, Fessi H. A pilot study of freeze drying of poly(epsilon-caprolactone) nanocapsules stabilized by poly(vinyl alcohol): formulation and process optimization. Int J Pharm 2006;309:178–88.
[27] Abdelwahed W, Degobert G, Stainmesse S, Fessi H. Freeze-drying of nanoparticles: formulation, process and storage considerations. Adv Drug Deliv Rev 2006;58(15):1688–713.
[28] Healy AM, Amaro MI, Paluch KJ, Tajber L. Dry powders for oral inhalation free of lactose carrier particles. Adv Drug Deliv Rev 2014;75:32–52.
[29] Nawaz A, Wong TW. Microwave as skin permeation enhancer for transdermal drug delivery of chitosan-5-fluorouracil nanoparticles. Carbohydr Polym 2017;157:906–19.
[30] Shi LJ, Li Z, Yu L, Jia H, Zheng LQ. Effects of surfactants and lipids on the preparation of solid lipid nanoparticles using double emulsion method. J Dispers Sci Technol 2011;32(2):254–9.
[31] Hiemenz PC, Rajagopalan R. The electrical double layer and double layer interactions. Principles of colloid and surface chemistry. 3rd ed. New York: Marcel Dekker; 1997. p. 499–533.
[32] Segal L, Creely JJ, Martin AE, Conrad CM. An empirical method for estimating the degree of crystallinity of native cellulose using the X-ray diffractometer. Textile Res J 1959;29(10):786–94.
[33] Vishu Kumar B, Varadaraj MC, Lalitha RG, Tharanathan RN. Low molecular weight chitosans: preparation with the aid of papain and characterization. Biochim Biophys Acta Gen Sub 2004;1670(2):137–46.
[34] Aerosols, nasal sprays, metered-dose inhalers, and dry powder inhalers. US Pharmacopeia 30-National Formulary, Chapter 601, 2007;25:225–45.
[35] Leane MM, Nankervis R, Smith A, Illum L. Use of the ninhydrin assay to measure the release of chitosan from oral solid dosage forms. Int J Pharm 2004;271(1–2):241–9.
[36] Varmuza K, Karlovits M, Demuth W. Spectral similarity versus structural similarity: infrared spectroscopy. Anal Chim Acta 2003;490(1–2):313–24.
[37] Dalmoro A, d'Amore M, Barba AA. Droplet size prediction in the production of drug delivery microsystems by ultrasonic atomization. Translational Medicine@UniSA 2013;7:6–11.
[38] Birdi KS. Introduction to surface and colloid chemistry: recent advances and general remarks. Handbook of surface and colloid chemistry. CRC Press; 2015. p. 1–144.
[39] Mohd Chachuli SH, Nawaz A, Shah K, Naharudin I, Wong TW. *In vitro* investigation of chitosan nanoparticles on fluorescein permeation into alveolar macrophages. Pharm Res 2016;33(6):1487–508.
[40] McNamee CE, Matsumoto M, Hartley PG, Hartley PG, Mulvaney P, Tsujii Y, et al. Interaction forces and zeta potentials of cationic polyelectrolyte coated silica surfaces in water and in ethanol: effects of chain length and concentration of perfluorinated anionic surfactants on their binding to the surface. Langmuir 2001;17(20):6220–7.
[41] Kouchak M, Avadi M, Abbaspour M, et al. Effect of different molecular weights of chitosan on preparation and characterization of insulin loaded nanoparticles by ion gelation method. Int J Drug Dev Res 2012;4(2):271–7.
[42] Abd Majid AM, Wong TW. Gas-pressurized dispersive powder flow tester for low volume sample characterization. Int J Pharm 2013;448:150–8.
[43] Chidavaenzi OC, Buckton G, Koosha F. The effect of co-spray drying with polyethylene glycol 4000 on the crystallinity and physical form of lactose. Int J Pharm 2001;216:43–9.
[44] Corrigan DO, Healy AM, Corrigan OI. The effect of spray drying solutions of polyethylene glycol (PEG) and lactose/PEG on their physicochemical properties. Int J Pharm 2002;235:193–205.
[45] Zhou Q, Morton DAV. Drug-lactose binding aspects in adhesive mixture: controlling performance in dry powder inhaler formulations by altering lactose carrier surfaces. Adv Drug Deliv Rev 2012;64:275–84.
[46] Kho K, Hadinoto K. Dry powder inhaler delivery of amorphous drug nanoparticles: effects of the lactose carrier particle shape and size. Powder Technol 2013;233:303–11.